Report

Neuron

Kinetics of Releasable Synaptic Vesicles and Their Plastic Changes at Hippocampal Mossy Fiber Synapses

Highlights

- We monitored exocytosis at mossy fiber boutons using electrophysiology and TIRF
- Priming of already-tethered vesicles determines fast vesicle replenishment
- cAMP, an important regulator of LTP, increases vesicular release probability
- cAMP likely changes the coupling between Ca^{2+} channels and synaptic vesicles

Authors

Mitsuharu Midorikawa, Takeshi Sakaba

Correspondence

midorikawa.mitsuharu@twmu.ac.jp (M.M.), tsakaba@mail.doshisha.ac.jp (T.S.)

In Brief

Midorikawa and Sakaba combined electrophysiological recordings and total internal reflection microscopy and revealed the dynamics of synaptic vesicles at hippocampal mossy fiber boutons in basal and cAMP-potentiated states, which may be relevant for LTP.

Midorikawa & Sakaba, 2017, Neuron *96*, 1033–1040
December 6, 2017
https://doi.org/10.1016/j.neuron.2017.10.016

CellPress

Neuron
Report

Kinetics of Releasable Synaptic Vesicles and Their Plastic Changes at Hippocampal Mossy Fiber Synapses

Mitsuharu Midorikawa[1,2,*] and Takeshi Sakaba[1,3,*]
[1]Graduate School of Brain Science, Doshisha University, Kyoto 6100394, Japan
[2]Department of Physiology, School of Medicine, Tokyo Women's Medical University, Tokyo 1628666, Japan
[3]Lead Contact
*Correspondence: midorikawa.mitsuharu@twmu.ac.jp (M.M.), tsakaba@mail.doshisha.ac.jp (T.S.)
https://doi.org/10.1016/j.neuron.2017.10.016

SUMMARY

Hippocampal mossy fiber boutons (hMFBs) are presynaptic terminals displaying various forms of synaptic plasticity. The presynaptic mechanisms underlying synaptic plasticity still remain poorly understood. Here, we have combined high temporal resolution measurements of presynaptic capacitance and excitatory postsynaptic currents (EPSCs) to measure the kinetics of exocytosis. In addition, total internal reflection fluorescence (TIRF) microscopy was employed to directly visualize dynamics of single synaptic vesicles adjacent to the plasma membrane at high spatial resolution. Readily releasable vesicles mostly consisted of already-tethered vesicles in the TIRF field. Vesicle replenishment had fast and slow phases, and TIRF imaging suggests that the fast phase depends on vesicle priming from already-tethered vesicles. Application of cyclic AMP (cAMP), a molecule crucial for LTP, mainly increases the vesicular release probability rather than the number of readily releasable vesicles or their replenishment rate, likely by changing the coupling between Ca^{2+} channels and synaptic vesicles. Thus, we revealed dynamic properties of synaptic vesicles at hMFBs.

INTRODUCTION

Synaptic transmission and plasticity are fundamental processes underlying our brain function. Extensive studies have been carried out to understand the detailed properties of these processes, but on the presynaptic side, our current knowledge is largely based on the highly detailed analysis from the few types of synapses, where direct recordings from the presynaptic terminal are feasible (Katz, 1969; von Gersdorff and Matthews, 1994; Forsythe, 1994; Geiger and Jonas, 2000; Ritzau-Jost et al., 2014). The properties of transmitter release have long been investigated by back calculation from the postsynaptic currents (Katz, 1969; Diamond and Jahr, 1995; Neher and Sakaba, 2001) or by measuring presynaptic surface membrane capacitance (von Gersdorff and Matthews, 1994; Sun and Wu, 2001; Hallermann et al., 2003). Moreover, transmitter release has been examined by imaging techniques (Betz and Bewick, 1992; Sankaranarayanan and Ryan, 2000; Zenisek et al., 2000; Midorikawa and Sakaba, 2015). In spite of recent advances in experimental techniques, the number of presynaptic terminals at which electrophysiological and imaging methods can be applied simultaneously is still largely limited to large synapses (Borst and Sakmann, 1996; Zenisek et al., 2000; Midorikawa et al., 2007; Ritzau-Jost et al., 2014). Hippocampal mossy fiber boutons (hMFBs) are large presynaptic terminals, which are amenable to both electrophysiological and imaging approaches (Geiger and Jonas, 2000). hMFBs are known to form synapses with CA3 pyramidal cells (Nicoll and Schmitz, 2005), and it is well known that short- and long-term plasticity at this synapse involves presynaptic mechanisms (Nicoll and Malenka, 1995). Therefore, hMFBs could be served as an interesting model of cortical synapses to reveal mechanisms of synaptic transmission and presynaptic plasticity.

Here, we dissociated hMFBs from transverse hippocampal slices, let the active zones adhere tightly to the glass coverslip, and visualized dynamics of single synaptic vesicles by total internal reflection fluorescence (TIRF) imaging with high spatial resolution. The net amount of exocytosis was examined simultaneously by applying capacitance measurement techniques. Moreover, the kinetics of transmitter release during the stimulation, which cannot be addressed directly by capacitance measurements, was examined closely on a sub-ms scale using paired recordings from hMFBs and CA3 pyramidal cells in acute slice preparations. These diverse and complementary approaches dissected the detailed kinetics of synaptic vesicles until they fuse with unprecedented spatiotemporal resolution.

Presynaptic forms of synaptic plasticity at this synapse, such as long-term potentiation and depression, involve Ca^{2+}- and cyclic AMP (cAMP)-dependent mechanisms (Nicoll and Malenka, 1995; Nicoll and Schmitz, 2005), though mechanistic insights through direct presynaptic recordings have not been obtained. To test the effect of cAMP-induced potentiation, we introduced cAMP directly into hMFBs through the patch pipette and examined the effects on exocytosis and pre-exocytotic vesicular activities. We reveal that an increase in the vesicular release probability, possibly by shortening the coupling distance

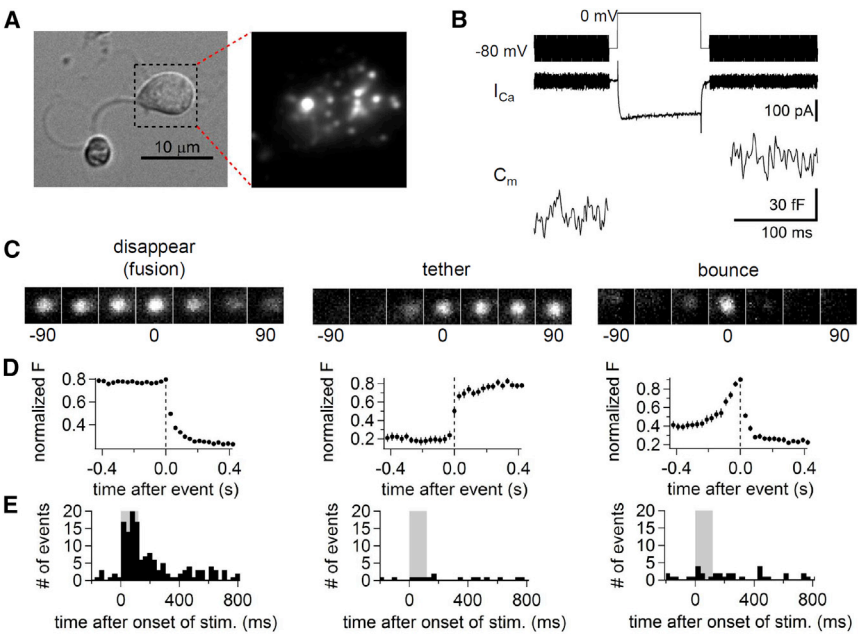

Figure 1. Whole-Cell Recordings and TIRF Imaging of FM-Labeled Synaptic Vesicles from Dissociated Hippocampal Mossy Fiber Boutons

(A) Images of an FM-loaded dissociated hippocampal mossy fiber bouton (hMFB) attached to a coverslip. Differential interference contrast (DIC) image (left) and TIRF image illuminated by 488-nm excitation laser (right) are shown.

(B) A depolarizing pulse (0 mV for 100 ms) was applied to elicit Ca^{2+} influx and exocytosis (top: command voltage; middle: Ca^{2+} current; bottom: capacitance).

(C) Example sequential images of "disappear (fusion)," "tether," and "bounce" events.

(D) Normalized fluorescence intensity was plotted against time. Spots were visible until time 0 for disappear and bounce. Tether spots were invisible before time 0.

(E) Peri-stimulus time histograms (PSTHs) of each type of event. 100-ms depolarizing pulses to 0 mV were applied at the time indicated by gray shading. No. of events: disappear 173, tether 17, and bounce 51; 92 sweeps from 36 cells.

See also Figure S1.

between Ca^{2+} channels and release-ready vesicles, is responsible for chemically induced potentiation at hMFBs.

RESULTS

TIRF Imaging of Single Synaptic Vesicles at the hMFBs

We acutely dissociated hMFBs (see STAR Methods) and plated the cell suspension onto coverslips (Figure 1A, left). Dissociated hMFBs were identified based on (1) their characteristic morphology (smooth spherical shape with 5∼10 μm diameter), (2) FM labeling, and (3) inward calcium current and capacitance jumps in responses to a depolarization pulse. To ensure visualization of individual synaptic vesicles (and to avoid imaging of overlapping, multiple synaptic vesicles), those were sparsely labeled by FM1–43 (<1%; Zenisek et al., 2000; Midorikawa and Sakaba, 2015). As observed in TIRF-based synaptic vesicle imaging studies (Zenisek et al., 2000; Midorikawa et al., 2007; Chen et al., 2013; Midorikawa and Sakaba, 2015), FM-loaded vesicles in close proximity to the plasma membrane (<100 nm) appeared as bright spots (Figure 1A, right). We only analyzed the spots with diffraction limited sizes, which have been assumed to be individual synaptic vesicles (Zenisek et al., 2000; Midorikawa and Sakaba, 2015). That stimulus-induced exocytosis occurs at dissociated hMFBs was confirmed by capacitance jumps in response to depolarizations (Figure 1B). FM-loaded dissociated hMFBs were voltage clamped, and 100-ms depolarizations were applied to evoke exocytosis during TIRF imaging of FM-labeled synaptic vesicles. Ca^{2+} imaging (using a Ca^{2+}-sensitive dye) showed punctate domains of increased Ca^{2+} concentrations in the TIRF footprint, indicating that Ca^{2+} channels are clustered at active zones after dissociation (Figure S1). Dynamics of the FM spots were classified into "disappear," "tether," and "bounce" events based on their time courses of fluorescence changes (Midorikawa and Sakaba, 2015; Figures 1C–1E; see STAR Methods). Some disappear events showed the diffusional spreading of the FM dye into the surrounding area prior to disappearance (Figure S1). Furthermore, the time course of fluorescence changes for disappear events as well as their stimulus dependence (Figures 1C–1E) suggested that these events represented exocytosis, as in previously reported TIRF imaging studies (Zenisek et al., 2000; Midorikawa et al., 2007; Chen et al., 2013; Midorikawa and Sakaba, 2015). There were far fewer tether and bounce events, and those showed weak stimulus dependence (Figures 1C–1E). Only a very small fraction of the bounce events (1 out of 37) showed a spreading of the dye that would be consistent with a fusion event. However, the fraction is too small and does not affect the overall conclusion; thus, we classified bounce events as non-fusion events.

Time Course of Exocytosis and the Readily Releasable Vesicle Pool Estimated from Capacitance Measurements

To dissect the kinetics of exocytosis at hMFBs with high time resolution, we performed analysis based on electrophysiological recordings from hMFBs in slices and in dissociated cells. hMFBs form synapses with CA3 pyramidal cells, and in slice preparations, pre- and postsynaptic paired recordings are feasible (Geiger and Jonas, 2000; Vyleta and Jonas, 2014). Upon stimulation of the presynaptic hMFB with a train of action potential (AP)-like depolarizations, excitatory postsynaptic currents (EPSCs) from the postsynaptic CA3 pyramidal cell showed prominent facilitation, a typical feature of hMFB-CA3 synapses (Salin et al., 1996; Figure 2A). EPSC amplitudes upon a single AP-like stimulus (36 ± 9 pA; similar to a quantal size; n = 3) indicate that a single AP-like stimulus triggers release of only 1 or 2 vesicles initially. To examine the characteristics of the readily releasable pool (RRP)

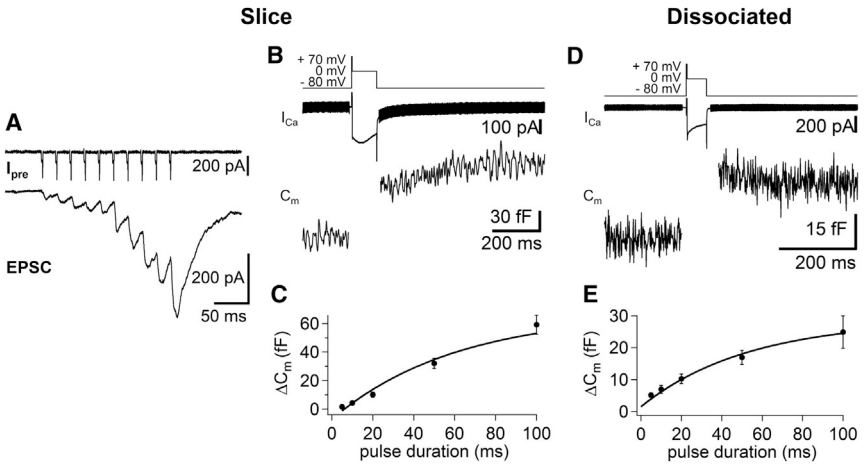

Figure 2. Depolarization-Induced Capacitance Jumps of hMFBs in Slices and after Dissociations

(A) Example traces of a paired recording in which the hMFB was stimulated in the voltage-clamp configuration with a train of AP-like stimulations (depolarization to 40 mV for 2 ms; 50 Hz; n = 3 cells), and recorded I_{Ca} was shown on top. An EPSC recorded from a CA3 pyramidal neuron was shown in the bottom.

(B) An example capacitance jump of the hMFB in a slice evoked by a depolarizing pulse (+70 mV for 2 ms followed by repolarization to 0 mV for 100 ms). (Top) Command voltage, (middle) Ca^{2+} current, and (bottom) capacitance are shown.

(C) The averaged capacitance jumps of the hMFBs in slices were plotted against the durations of depolarizations (n = 5–12).

(D) An example capacitance jump of the dissociated hMFB evoked by a depolarizing pulse (+70 mV for 2 ms followed by repolarization to 0 mV for 50 ms). (Top) Command voltage, (middle) Ca^{2+} current, and (bottom) capacitance are shown.

(E) The amount of capacitance jumps of the dissociated hMFBs was plotted against the durations of depolarizations (n = 10–14).

of synaptic vesicles, capacitance jumps of the hMFBs were recorded in response to various durations of presynaptic voltage depolarizations in acute slices (Figures 2B and 2C). The RRP size estimated from capacitance jumps (~50 fF) was in good agreement with previous work (Hallermann et al., 2003). The time course of the RRP release was fitted by a single exponential with $\tau = 61$ ms (Figure 2C). The same protocol was applied to the dissociated hMFBs, and the capacitance jumps in response to variable durations of depolarizations are shown in Figures 2D and 2E. The estimated RRP size of the dissociated hMFBs was smaller (~30 fF) than in slices, possibly because of the dissociation procedure (Midorikawa and Sakaba, 2015). The time course of the RRP release (56.5 ms; Figure 2E) was in good agreement with the slice data, though the dissociated cell data might indicate a fast-releasing component during a few ms after the onset of depolarizing pulse (Hallermann et al., 2003). These results show that, although the RRP size is smaller after dissociations, the time course of the RRP release remains similar to that in slices. The smaller AP-induced EPSC and the lack of fast release component in case of the slice preparation compared with the previous study (Hallermann et al., 2003; and also with dissociated hMFBs data in this study) might be caused by higher concentration of EGTA (0.5 mM) as well as high access resistance, because the activation time constant of the calcium current was 2.67 ± 0.31 ms for slice hMFBs and 0.62 ± 0.11 ms for dissociated hMFBs.

Time Course of Exocytosis and Synaptic Vesicle Replenishment Measured from Paired Recordings of hMFB and CA3 Pyramidal Cell

The amplitudes of capacitance jumps reflect the total change of membrane surface following the depolarization. However, because membrane capacitance cannot be measured during the depolarization, the time course of exocytosis cannot be investigated. Also, capacitance measurements may include exocytosis of dense core granules and may be compromised by ongoing endocytosis, which may confound our estimation of synaptic vesicle fusion. Thus, in addition to capacitance measurements, we assessed the time course of exocytosis with sub-ms time resolution from postsynaptic responses. In paired recordings from the hMFB-CA3 pyramidal cell synapse, we simultaneously measured the total amount of exocytosis via presynaptic capacitance measurements and the time course of exocytosis during the depolarization via analyses of EPSCs (Figure 3A). The time course of exocytosis was calculated by EPSC deconvolution with miniature EPSCs (mEPSCs) (postsynaptic responses to single synaptic vesicle release events), which provides the vesicle release rate (Diamond and Jahr, 1995; Neher and Sakaba, 2001). Integrating this release rate provides the cumulative number of vesicles released at a given time after the stimulus. This revealed a rather slow time course of exocytosis during the pulse (Figure 3B; pulse timing is shown by a gray shading, fitted by a single exponential with a time constant of 36 ms). This is consistent with capacitance measurements, in which the time course of RRP release has a slow time constant of tens of ms (Figures 2C and 2E). Deconvolution analysis also revealed the copious asynchronous release after the depolarization. The RRP size estimated from the deconvolution method was ~400 vesicles. This agrees well with the capacitance measurement, because long (i.e., RRP-depleting) depolarizations induced a capacitance jump of ~50 fF. Considering a capacitance jump per single vesicle fusion of 100 aF (which depends on the vesicle diameter), this corresponds to an RRP size of ~500 vesicles. Additionally, the slightly higher estimate from capacitance measurements may reflect some vesicles fusing toward interneurons or dense core vesicle fusion. The copious asynchronous release observed is consistent with previous work showing a loose coupling between Ca^{2+} channels and release sensors at hMFBs (Vyleta and Jonas, 2014). The time course of exocytosis can also be estimated by TIRF imaging as the time course of disappearance events. This time course (Figure 3C) is in good agreement with that of release rates calculated from EPSC deconvolution (Figure 3B), further arguing that our classification of disappear events as exocytosis is justified. The number of TIRF-measured disappear events decreased from 19 (immediately) to 1 (10 min) after the start of whole-cell

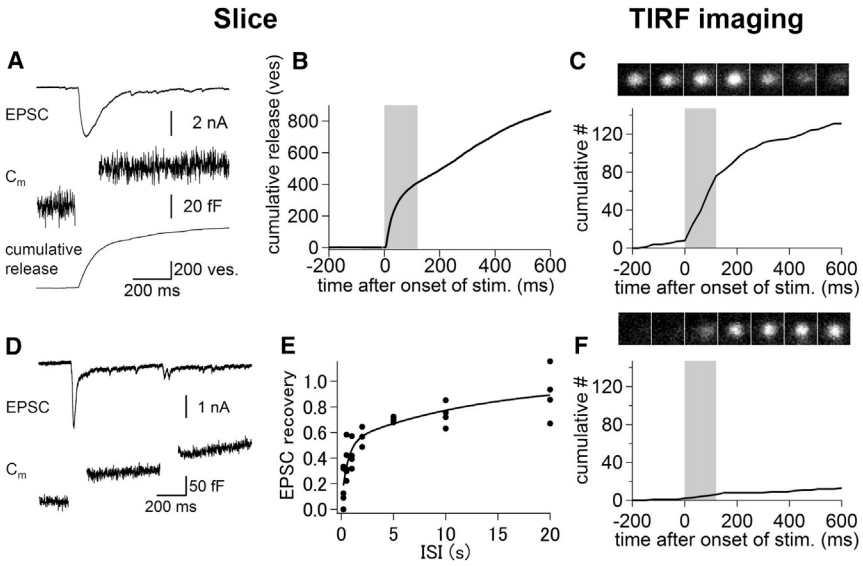

Figure 3. Time Course of Exocytosis and Vesicle Replenishment Measured by Electrophysiology and TIRF Imaging

(A) Example EPSC (top) and capacitance (middle) traces from a postsynaptic CA3 pyramidal cell and a presynaptic hMFB paired recording in a slice preparation, respectively. A 100-ms depolarization to 0 mV was applied to the hMFB to evoke exocytosis. Cumulative release from the deconvolution method is shown in bottom.

(B) Average plot of cumulative release rate induced by 100-ms depolarizations (n = 9 pairs). A 100-ms depolarizing pulse to 0 mV was applied at the time indicated by gray shading.

(C) A cumulative plot of disappear events observed by TIRF imaging. A 100-ms depolarizing pulse to 0 mV was applied at the time indicated by gray shading.

(D) Two depolarization pulses (0 mV for 100 ms) were applied with various inter-stimulus intervals (ISIs). An EPSC trace from a postsynaptic CA3 pyramidal cell (top) and a capacitance trace from a presynaptic hMFB (bottom) are shown.

(E) The amount of EPSC recovery (cumulative release) was plotted against ISI (n = 6 pairs).

(F) A cumulative plot of tether events observed by TIRF imaging. The datasets in (C) and (F) are the same as in Figure 1E.

See also Figure S2.

recording with 100 nM tetanus toxin included in the patch pipette, but bounce events were not blocked (12 and 18 immediately after and 10 min after tetanus toxin infusion; 11 cells), suggesting that stimulated exocytosis, but not bouncing, depends on SNARE pairing/assembly.

We next examined the recovery of the RRP after depletion at the hMFBs by applying pairs of pool-depleting 100-ms depolarization pulses at various inter-stimulus intervals in slices (Figure 3D). The recovery was measured both by capacitance measurements and by EPSC recordings, and we confirmed that the recovery of C_m and the cumulative release after deconvolution or EPSC amplitude showed a linear relationship, suggesting that the deconvolution is valid under our experimental condition (Figure S2). In Figure 3E, the recovery of EPSC was plotted against inter-stimulus intervals. The time course of the RRP recovery was fitted by a double exponential, which suggests that the RRP of hMFBs is replenished with a fast component that has a time constant of 600 ms followed by a slow component with a time constant of 13 s (Figure 3E; n = 6 pairs). If the recruitment of vesicles from the cytosol to the membrane was the rate-limiting step in synaptic vesicle replenishment, then replenishment is expected to correlate with the tethering of new vesicles. In that case, replenishment should be reflected by translocation of labeled vesicles toward the plasma membrane and subsequent stabilization in TIRF imaging (i.e., tethering of vesicles to the plasma membrane; Figure 3F). Thus, we examined whether RRP replenishment can be supported by such newly tethered vesicles or not. By comparing the time course of tether events with the number of disappear events during the stimulation (i.e., RRP size), we estimated that tether events could refill the RRP with a time constant of 4.9 s. These data indicate that the tethering rates are too slow to explain the fast replenishment of RRP. The time constant of tether events to refill the RRP was more consistent with the slow component of the RRP recovery measured from electrophysiology. Fast replenishment may not rely on the physical movements of the synaptic vesicles toward the plasma membrane, but rather they may be mediated by the molecular priming of already-tethered vesicles. Consistently, when a pair of 100 ms depolarizing pulse (ISI = 2 s) was applied, the number of disappear events evoked by the second pulse was 53.8% of those evoked by first pulse (28 versus 52), and 78.6% (22 out of 28) disappear events evoked by the second pulse was mediated by already-tethered vesicles before the first pulse (53 sweeps from 19 cells).

Effects of cAMP-Induced Potentiation on the Kinetics of Exocytosis

hMFBs are known to have a notable characteristic that long-term potentiation (LTP) induction involves a largely presynaptic mechanism (Nicoll and Malenka, 1995), and pharmacological and genetic analyses have revealed that a rise in presynaptic cAMP is a crucial component (Huang et al., 1994; Weisskopf et al., 1994). Thus, we induced "chemical LTP" by adding 0.5 mM cAMP in the patch pipette and investigated the effect of cAMP on the hMFB transmitter release. When cAMP (0.5 mM) was introduced into the dissociated hMFB through a patch pipette, the RRP size (determined by long-lasting depolarizations) remained constant, but the capacitance jumps in response to short depolarizations were increased (Figures 4A and 4B). As was previously shown, cAMP did not alter the amplitude of Ca^{2+} currents (Figure S3; Regehr and Tank, 1991; Kamiya et al., 2002; but see Lonart et al., 1998), which suggests that increase in the amount of exocytosis involves enhanced coupling of Ca^{2+} to exocytosis. The plot of capacitance jumps against Q_{Ca} further supports this idea (Figure S3). The effect of intracellular cAMP application was indistinguishable from that of extracellular forskolin application

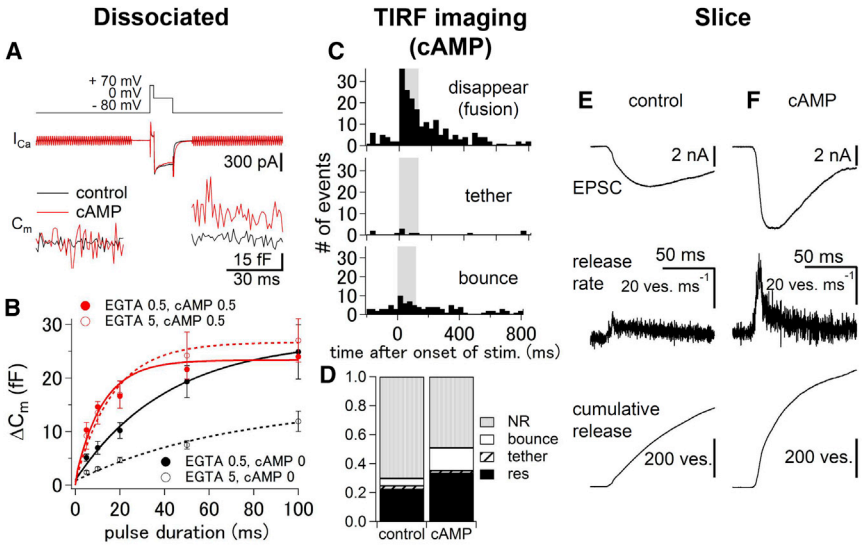

Figure 4. Effect of cAMP on the Time Course of Exocytosis

(A) Example traces in response to a 10-ms depolarization in control (black) and in cAMP (red) condition from dissociated hMFBs. (Top) Command voltage, (middle) Ca^{2+} current, and (bottom) capacitance are shown.

(B) The ΔCm of the dissociated hMFBs were plotted against the durations of depolarizations for EGTA 0.5 mM, cAMP 0 mM in the patch pipette (black filled circle; n = 10–14); EGTA 5 mM, cAMP 0 mM (black open circle; n = 9–13); EGTA 0.5 mM, cAMP 0.5 mM (red filled circle; n = 9–13); and EGTA 5 mM, cAMP 0.5 mM (red open circle; n = 7).

(C) PSTHs of each type of event observed by TIRF imaging in cAMP condition. 100-ms depolarizing pulses to 0 mV were applied at the time indicated by gray shadings (no. of events; disappear 276, tether 16, and bounce 203; 90 sweeps from 23 cells).

(D) Relative proportions of "responder" (res), tether, bounce, and "nonresponder" (NR) events are shown for control and cAMP conditions. The fraction of disappear events was somewhat higher in cAMP condition, but not statistically significant, mainly because of the large fluctuations caused by small event numbers for each sweep/cell.

(E and F) Simultaneous pre- and postsynaptic recordings were performed, and the release rates were calculated by deconvolution of EPSCs with the mEPSCs. A 100-ms depolarizing pulse to 0 mV was applied to the hMFBs, and the EPSCs were recorded from the CA3 pyramidal cells. Example traces are shown. Addition of cAMP in the patch pipette (0.5 mM) potentiated the peak release rates: peak release rates were 14.7 ± 3.8 vesicles ms^{-1} (control; n = 9 cell pairs; E) and 35.5 ± 5.9 vesicles ms^{-1} (cAMP; n = 4 cell pairs; F), respectively ($p < 0.02$). The cumulative release during the pulse (RRP) was 446 ± 116 vesicles (control) and 870 ± 197 vesicles (cAMP), respectively ($p > 0.05$). From top, EPSC, release rate, and cumulative release in an example cell pair are shown.

See also Figures S3 and S4.

(Figure S3). As the downstream target of cAMP-induced exocytosis facilitation, protein kinase A (PKA) has been suggested (Weisskopf et al., 1994); thus, we blocked the activity of PKA by an application of KT5720. The effect of cAMP was abolished by an application of KT5720 (Figure S3), suggesting that PKA is the downstream target of cAMP for hMFB exocytosis facilitation. The enhancement of exocytosis in response to shorter depolarizations induced by cAMP application was also observed in hMFBs in slices (Figure S4). Specifically, release rate constant was increased to 250%, and the RRP sizes were increased by 30%–40% (no significance when comparing C_m jumps at 100 ms). Although we cannot exclude the possibility of a moderate increase in the RRP size, the main effect of cAMP was a change in the Ca^{2+} sensitivity of vesicle fusion. Consistently, forskolin increased the AP-induced EPSCs and decreased the paired-pulse ratio at the CA3 pyramidal cell (Figure S4).

The enhanced Ca^{2+} sensitivity could be caused by (1) tighter coupling between Ca^{2+} channels to vesicles or (2) higher intracellular Ca^{2+} sensitivity of the vesicles. Loose and tight coupling between Ca^{2+} channels and vesicles can be distinguished by sensitivity to EGTA, because EGTA predominantly blocks loosely coupled vesicles (Borst and Sakmann, 1996). Therefore, if EGTA is less effective in blocking release in the presence of cAMP, it suggests that the coupling distances may become tighter. Capacitance jumps were strongly inhibited by 5 mM EGTA in the absence of cAMP in the intracellular solution but were not affected when 0.5 mM cAMP was induced together with 5 mM EGTA (Figure 4B). 5 mM 1,2-bis(*o*-aminophenoxy) ethane-*N*,*N*,*N*′,*N*′-tetraacetic acid (BAPTA) blocked capacitance jumps irrespective of cAMP (n = 3 each). The results suggest that cAMP tightens the coupling between Ca^{2+} channels and release-ready synaptic vesicles.

We next examined the mechanism of cAMP-induced potentiation by TIRF imaging. Dissociated hMFBs were loaded with FM dye and infused with 0.5 mM cAMP through a patch pipette before exocytosis was evoked by a single 100-ms depolarization pulse. Vesicle dynamics were again classified into three types (disappear, tether, and bounce; Figure 4C). We furthermore included "nonresponder" (NR) events, which stayed stationary at the plasma membrane throughout the recordings. When we compared the proportion of each type of event with and without cAMP, we found that the fraction of disappear events was somewhat higher in cAMP condition (Figure 4D; not statistically significant). Most notably, the time course of disappear events during the pulse got faster by adding cAMP (Figure 4C). After the onset of depolarization (first frame after depolarization), the frequency of disappear events was higher in the presence of cAMP ($p < 0.05$, compared with control condition; compare Figures 4C and 1E; see also Figure S4). This is consistent with the results showing that cAMP enhanced the exocytosis induced by shorter depolarizations (Figure 4B), suggesting that cAMP changes sensitivity of releasable synaptic vesicles to Ca^{2+} influx. Detailed analysis of release rates with the higher temporal resolution of paired recordings further indicated that cAMP enhanced the rapid component of exocytosis (Figures 4E and 4F), consistent with a change in the sensitivity of vesicles to Ca^{2+} influx (see Discussion). In TIRF imaging, the tethering rate was unchanged, suggesting that the speed of slow vesicle replenishment was not affected by cAMP (Figure 4C; see also Figure S2). The rate of bounce events increased by cAMP (Figure 4D), but because

we found no direct correlation between increased bounce events and fusion dynamics, we did not investigate this further.

DISCUSSION

This is the first study to examine spatiotemporal dynamics of synaptic vesicles in hMFBs directly. We show that RRP vesicles mostly consist of vesicles stably tethered within the TIRF field at the plasma membrane before stimulus onset. Tethering rates were slow, and newly tethered vesicles could not participate in exocytosis immediately. In addition, cAMP, an important regulator of LTP at hMFBs, likely enhances vesicular release probability by changing the coupling distance between Ca^{2+} channels and RRP vesicles.

Our results confirm a remarkably large RRP size in hMFBs (Hallermann et al., 2003). RRP estimates from capacitance measurements rely on an estimation of the capacitance jump caused by a single vesicle fusion event. Also, the capacitance jumps may include dense corevesicle fusion and vesicle fusion toward interneurons. Nevertheless, a linear relationship between capacitance jumps and cumulative release from EPSC deconvolution (Figure S2) confirms overall validity of capacitance measurements. A large RRP is consistent with a large number of docked vesicles at hMFBs active zones (~900 vesicles or ~40 vesicles per active zone; Rollenhagen et al., 2007) and also fits well with the functional demand on hMFBs, which exhibit unusually low overall firing rates but high-frequency activity during burst firing (Jung and McNaughton, 1993).

Another distinct feature of hMFBs is the slow tethering of new vesicles from the cytosolic region to the plasma membrane. It has been controversial whether vesicle tethering or priming is rate limiting (Kaeser and Regehr, 2017). In ribbon synapses and cerebellar mossy fiber synapses (Zenisek et al., 2000; Saviane and Silver, 2006; Rothman et al., 2016), biophysical measurements suggest that the RRP is relatively small and that rapid vesicle tethering is required for sustained release. In this case, vesicle priming should be so fast that it is not rate limiting for fusion during repetitive activity. In contrast, other studies mainly using electron microscopy and genetics rather suggest that priming could be rate limiting (Imig et al., 2014; Kaeser and Regehr, 2017). Our results from hMFBs suggest that vesicle tethering is too slow to explain rapid synaptic vesicle replenishment to the RRP. In addition, the double-pulse experiment in TIRF imaging suggests that fast vesicle replenishment is mediated by the transition of already tethered vesicles into a release-ready state, similar to the situation at the calyx of Held (Midorikawa and Sakaba, 2015). Under physiological conditions, the RRP of hMFBs is hardly depleted because of a low vesicular release probability. Likewise, at the calyx of Held, release probability is not as high as at cerebellar and ribbon synapses (Schneggenburger et al., 2002). We suggest that active zone scaffolds are constructed differently depending on the demand of vesicle supply.

cAMP has been shown to be responsible for long-term plasticity at hMFBs (Nicoll and Malenka, 1995), but the underlying mechanism remains unsolved. Previous studies suggest that cAMP augments the RRP, Ca^{2+} influx, and vesicular release probability (Lonart et al., 1998). In addition, physiological studies have suggested an increase in the number of functional release sites during LTP (Reid et al., 2004; Chamberland et al., 2014). By introducing cAMP into the hMFBs through the patch pipette, we provide direct evidence that increased vesicular release probability is mainly responsible for cAMP-induced potentiation. Enhancement of Ca^{2+} influx via modulation of voltage-gated calcium channels have been shown to play a role in LTP in some synapses (Lonart et al., 1998), but our results show this is not the case at hMFBs, consistent with previous reports (Regehr and Tank, 1991; Kamiya et al., 2002). RRP size remained unchanged or increased modestly (if at all), which speaks against an increase in the number of release sites (Reid et al., 2004). Furthermore, TIRF measurements only revealed a modest increase (if any) in the number of tethered or releasable vesicles. These findings can be reconciled by postulating that the release probability is so low that some release sites behave as silent sites in the basal condition (Chamberland et al., 2014). The increased Ca^{2+} sensitivity observed upon cAMP treatment may either involve a change in the Ca^{2+} sensitivity of vesicle fusion (superpriming; Schlüter et al., 2006; Lee et al., 2013) or a change in the coupling distance between Ca^{2+} channels and synaptic vesicles within the release site (positional priming; Wadel et al., 2007). Our results suggest that tighter channel-vesicle coupling or positional priming can be the mechanism of plasticity. A target of cAMP/PKA remains unknown. Several molecules, such as RIM, Rab3, Munc13, and synaptotagmin12, have been postulated as important elements for LTP (Castillo et al., 1997, 2002; Yang and Calakos, 2011; Kaeser-Woo et al., 2013).

We should note several caveats of this study. Dissociated terminals may be different from intact ones, and release sites directly attached to the coverslip that are used in the TIRF experiments may somewhat differ from those that are not facing the coverslip. Nevertheless, we unraveled the kinetics of synaptic vesicle tethering and docking/priming in hMFBs, which may be the first step toward a mechanistic understanding of short- and long-term presynaptic plasticity, a prominent feature of these presynaptic terminals.

STAR★METHODS

Detailed methods are provided in the online version of this paper and include the following:

- KEY RESOURCES TABLE
- CONTACT FOR REAGENTS AND RESOURCE SHARING
- EXPERIMENTAL MODEL AND SUBJECT DETAILS
  - Rats
- METHOD DETAILS
  - Slice, FM-loading, and cell dissociation
  - Whole-cell recordings
  - TIRF microscopy
  - Analysis
- QUANTIFICATION AND STATISTICAL ANALYSES

SUPPLEMENTAL INFORMATION

Supplemental Information includes four figures and can be found with this article online at https://doi.org/10.1016/j.neuron.2017.10.016.

AUTHOR CONTRIBUTIONS

M.M. and T.S. designed research, conducted the experiments, and wrote the paper.

ACKNOWLEDGMENTS

We thank Martin Müller, Alexander Walter, and Shin-ya Kawaguchi for critical reading of the manuscript and helpful comments and Rinako Miyano for technical support. This work was supported by JSPS/MEXT KAKENHI grant numbers 15K18346, 17K19466, 17H03548 (M.M.), 15K14321, 15H04261, and 17H05753 (T.S.); Takeda Science Foundation (T.S.); and JSPS Core-to-Core Program A Advanced Research Networks.

Received: May 18, 2017
Revised: September 11, 2017
Accepted: October 10, 2017
Published: November 2, 2017

REFERENCES

Betz, W.J., and Bewick, G.S. (1992). Optical analysis of synaptic vesicle recycling at the frog neuromuscular junction. Science *255*, 200–203.

Borst, J.G., and Sakmann, B. (1996). Calcium influx and transmitter release in a fast CNS synapse. Nature *383*, 431–434.

Castillo, P.E., Janz, R., Südhof, T.C., Tzounopoulos, T., Malenka, R.C., and Nicoll, R.A. (1997). Rab3A is essential for mossy fibre long-term potentiation in the hippocampus. Nature *388*, 590–593.

Castillo, P.E., Schoch, S., Schmitz, F., Südhof, T.C., and Malenka, R.C. (2002). RIM1α is required for presynaptic long-term potentiation. Nature *415*, 327–330.

Chamberland, S., Evstratova, A., and Tóth, K. (2014). Interplay between synchronization of multivesicular release and recruitment of additional release sites support short-term facilitation at hippocampal mossy fiber to CA3 pyramidal cells synapses. J. Neurosci. *34*, 11032–11047.

Chen, M., Van Hook, M.J., Zenisek, D., and Thoreson, W.B. (2013). Properties of ribbon and non-ribbon release from rod photoreceptors revealed by visualizing individual synaptic vesicles. J. Neurosci. *33*, 2071–2086.

Diamond, J.S., and Jahr, C.E. (1995). Asynchronous release of synaptic vesicles determines the time course of the AMPA receptor-mediated EPSC. Neuron *15*, 1097–1107.

Forsythe, I.D. (1994). Direct patch recording from identified presynaptic terminals mediating glutamatergic EPSCs in the rat CNS, in vitro. J. Physiol. *479*, 381–387.

Geiger, J.R.P., and Jonas, P. (2000). Dynamic control of presynaptic $Ca^{(2+)}$ inflow by fast-inactivating $K^{(+)}$ channels in hippocampal mossy fiber boutons. Neuron *28*, 927–939.

Gillis, K.D. (2000). Admittance-based measurement of membrane capacitance using the EPC-9 patch-clamp amplifier. Pflugers Arch. *439*, 655–664.

Hallermann, S., Pawlu, C., Jonas, P., and Heckmann, M. (2003). A large pool of releasable vesicles in a cortical glutamatergic synapse. Proc. Natl. Acad. Sci. USA *100*, 8975–8980.

Huang, Y.Y., Li, X.C., and Kandel, E.R. (1994). cAMP contributes to mossy fiber LTP by initiating both a covalently mediated early phase and macromolecular synthesis-dependent late phase. Cell *79*, 69–79.

Imig, C., Min, S.W., Krinner, S., Arancillo, M., Rosenmund, C., Südhof, T.C., Rhee, J., Brose, N., and Cooper, B.H. (2014). The morphological and molecular nature of synaptic vesicle priming at presynaptic active zones. Neuron *84*, 416–431.

Jung, M.W., and McNaughton, B.L. (1993). Spatial selectivity of unit activity in the hippocampal granular layer. Hippocampus *3*, 165–182.

Kaeser, P.S., and Regehr, W.G. (2017). The readily releasable pool of synaptic vesicles. Curr. Opin. Neurobiol. *43*, 63–70.

Kaeser-Woo, Y.J., Younts, T.J., Yang, X., Zhou, P., Wu, D., Castillo, P.E., and Südhof, T.C. (2013). Synaptotagmin-12 phosphorylation by cAMP-dependent protein kinase is essential for hippocampal mossy fiber LTP. J. Neurosci. *33*, 9769–9780.

Kamiya, H., Umeda, K., Ozawa, S., and Manabe, T. (2002). Presynaptic Ca^{2+} entry is unchanged during hippocampal mossy fiber long-term potentiation. J. Neurosci. *22*, 10524–10528.

Katz, B. (1969). The Release of Neural Transmitter Substances (Liverpool, U.K.: Liverpool University Press).

Lee, J.S., Ho, W.K., Neher, E., and Lee, S.H. (2013). Superpriming of synaptic vesicles after their recruitment to the readily releasable pool. Proc. Natl. Acad. Sci. USA *110*, 15079–15084.

Lonart, G., Janz, R., Johnson, K.M., and Südhof, T.C. (1998). Mechanism of action of rab3A in mossy fiber LTP. Neuron *21*, 1141–1150.

Midorikawa, M., and Sakaba, T. (2015). Imaging exocytosis of single synaptic vesicles at a fast CNS presynaptic terminal. Neuron *88*, 492–498.

Midorikawa, M., Tsukamoto, Y., Berglund, K., Ishii, M., and Tachibana, M. (2007). Different roles of ribbon-associated and ribbon-free active zones in retinal bipolar cells. Nat. Neurosci. *10*, 1268–1276.

Neher, E., and Sakaba, T. (2001). Combining deconvolution and noise analysis for the estimation of transmitter release rates at the calyx of held. J. Neurosci. *21*, 444–461.

Nicoll, R.A., and Malenka, R.C. (1995). Contrasting properties of two forms of long-term potentiation in the hippocampus. Nature *377*, 115–118.

Nicoll, R.A., and Schmitz, D. (2005). Synaptic plasticity at hippocampal mossy fibre synapses. Nat. Rev. Neurosci. *6*, 863–876.

Regehr, W.G., and Tank, D.W. (1991). The maintenance of LTP at hippocampal mossy fiber synapses is independent of sustained presynaptic calcium. Neuron *7*, 451–459.

Reid, C.A., Dixon, D.B., Takahashi, M., Bliss, T.V., and Fine, A. (2004). Optical quantal analysis indicates that long-term potentiation at single hippocampal mossy fiber synapses is expressed through increased release probability, recruitment of new release sites, and activation of silent synapses. J. Neurosci. *24*, 3618–3626.

Ritzau-Jost, A., Delvendahl, I., Rings, A., Byczkowicz, N., Harada, H., Shigemoto, R., Hirrlinger, J., Eilers, J., and Hallermann, S. (2014). Ultrafast action potentials mediate kilohertz signaling at a central synapse. Neuron *84*, 152–163.

Rollenhagen, A., Sätzler, K., Rodríguez, E.P., Jonas, P., Frotscher, M., and Lübke, J.H. (2007). Structural determinants of transmission at large hippocampal mossy fiber synapses. J. Neurosci. *27*, 10434–10444.

Rothman, J.S., Kocsis, L., Herzog, E., Nusser, Z., and Silver, R.A. (2016). Physical determinants of vesicle mobility and supply at a central synapse. eLife *5*, e15133.

Salin, P.A., Scanziani, M., Malenka, R.C., and Nicoll, R.A. (1996). Distinct short-term plasticity at two excitatory synapses in the hippocampus. Proc. Natl. Acad. Sci. USA *93*, 13304–13309.

Sankaranarayanan, S., and Ryan, T.A. (2000). Real-time measurements of vesicle-SNARE recycling in synapses of the central nervous system. Nat. Cell Biol. *2*, 197–204.

Saviane, C., and Silver, R.A. (2006). Fast vesicle reloading and a large pool sustain high bandwidth transmission at a central synapse. Nature *439*, 983–987.

Schlüter, O.M., Basu, J., Südhof, T.C., and Rosenmund, C. (2006). Rab3 superprimes synaptic vesicles for release: implications for short-term synaptic plasticity. J. Neurosci. *26*, 1239–1246.

Schneggenburger, R., Sakaba, T., and Neher, E. (2002). Vesicle pools and short-term synaptic depression: lessons from a large synapse. Trends Neurosci. *25*, 206–212.

Sun, J.Y., and Wu, L.G. (2001). Fast kinetics of exocytosis revealed by simultaneous measurements of presynaptic capacitance and postsynaptic currents at a central synapse. Neuron *30*, 171–182.

von Gersdorff, H., and Matthews, G. (1994). Dynamics of synaptic vesicle fusion and membrane retrieval in synaptic terminals. Nature *367*, 735–739.

Vyleta, N.P., and Jonas, P. (2014). Loose coupling between Ca^{2+} channels and release sensors at a plastic hippocampal synapse. Science *343*, 665–670.

Wadel, K., Neher, E., and Sakaba, T. (2007). The coupling between synaptic vesicles and Ca^{2+} channels determines fast neurotransmitter release. Neuron *53*, 563–575.

Weisskopf, M.G., Castillo, P.E., Zalutsky, R.A., and Nicoll, R.A. (1994). Mediation of hippocampal mossy fiber long-term potentiation by cyclic AMP. Science *265*, 1878–1882.

Yang, Y., and Calakos, N. (2011). Munc13-1 is required for presynaptic long-term potentiation. J. Neurosci. *31*, 12053–12057.

Zenisek, D., Steyer, J.A., and Almers, W. (2000). Transport, capture and exocytosis of single synaptic vesicles at active zones. Nature *406*, 849–854.

STAR★METHODS

KEY RESOURCES TABLE

REAGENT or RESOURCE	SOURCE	IDENTIFIER
Chemicals, Peptides, and Recombinant Proteins		
SynaptoGreen C4 (FM1-43)	Biotium	Cat#70022; RRID: CVCL_DL71
TTX	Wako	Cat#206-11071
TEA-Cl	Sigma	Cat#T2265
D-AP5	Tocris	Cat#0106; RRID: IMSR_JAX:003333
CTZ	Tocris	Cat#0713; RRID: IMSR_JAX:003333
Forskolin	Wako	Cat#067-02191; RRID: IMSR_JAX:003333
Oregon Green 488 BAPTA-6F	Molecular Probes	Cat#023990; RRID: IMSR_JAX:003333
Tetanus Toxin	Funakoshi	Cat#190B; RRID: IMSR_JAX:003333
UBP310	Tocris	Cat#3621; RRID: IMSR_JAX:003333
Experimental Models: Organisms/Strains		
Wistar rats	Shimizu laboratory supplies, Japan SLC	N/A
Software and Algorithms		
IgorPro	Wavemetrics	N/A
Solis	Andor	N/A
Metamorph	Moleculardevices	N/A
Excel	Microsoft	N/A
MATLAB	MathWorks	N/A

CONTACT FOR REAGENTS AND RESOURCE SHARING

Further information and requests for resources and reagents should be directed to and will be fulfilled by the Lead Contact, Takeshi Sakaba (tsakaba@mail.doshisha.ac.jp)

EXPERIMENTAL MODEL AND SUBJECT DETAILS

Rats

Male and female Wister rats (postnatal days 21-30) were used in accordance with the guidelines of the Physiological Society of Japan. All procedures and animal cares were conducted in accordance with the guidelines of the Physiological Society of Japan, and were approved by Doshisha University committee for Regulation on the Conduct of Animal Experiments and Related Activities. All efforts were taken to minimize animal numbers.

METHOD DETAILS

Slice, FM-loading, and cell dissociation

Male and female Wister rats (postnatal days 21-30) were deeply anesthetized with isoflurane, decapitated, and brains were removed in accordance with the guidelines of the Physiological Society of Japan. 300 μm thick transverse hippocampus slices were obtained using a Leica VT1200S slicer (Leica Microsystems, Germany) in ice-cold slice medium contained (in mM) 87 NaCl, 75 sucrose, 25 $NaHCO_3$, 1.25 NaH_2PO_4, 2.5 KCl, 10 glucose, 0.5 $CaCl_2$ and 7 $MgCl_2$ (Hallermann et al., 2003). Slices were then incubated at 37°C for > 0.5 hr in a slice medium gassed with 95% O_2 and 5% CO_2. For slice electrophysiological recordings, slices were visualized on an upright microscope (BX-51, Olympus) in slice recording solution contained (in mM) 125 NaCl, 2.5 KCl, 25 glucose, 25 $NaHCO_3$, 1.25 NaH_2PO_4, 0.4 ascorbic acid, 3 myoinositol, 2 Na-pyruvate, 2 $CaCl_2$, 1 $MgCl_2$ (pH 7.4, gassed with 95% O_2 and 5% CO_2).

For FM-loading, slices were moved after incubation to a FM loading solution containing (in mM) 95 NaCl, 32.5 KCl, 25 glucose, 25 $NaHCO_3$, 1.25 NaH_2PO_4, 0.4 ascorbic acid, 3 myoinositol, 2 Na-pyruvate, 2 $CaCl_2$, 1 $MgCl_2$ and 0.01 FM1-43 for 1 min. Loading time was adjusted appropriately to label the vesicles sparse enough to visualize individual single vesicles under TIRF. After dissecting

unnecessary regions, the slices were digested in a cysteine (5 mM)-activated papain (1.25-5 mg/ml) added slice medium for 15-30 min at 37°C, rinsed and mechanically triturated with a fire polished Pasteur pipette (open diameter of 1 mm) in the slice medium. A few drops of cell suspension were plated on a glass-bottom dish (D111300, Matsunami Glass), coated with Concanavalin A. Cells were allowed to settle on the dish for 15 min. The solution was then replaced to dissociation recording medium contained (in mM) 125 NaCl, 2.5 KCl, 25 glucose, 25 HEPES, 1.25 NaH_2PO_4, 0.4 ascorbic acid, 3 myoinositol, 2 Na-pyruvate, 5 $CaCl_2$ (pH 7.3, 320 mosM). The solution was not perfused or bubbled during the recording, because solution exchange and bubbling caused possible movements, which may distort TIRF imaging. Dissociated hMFBs were identified based on (1) their characteristic morphology (smooth spherical shape with 5 ~10 μm diameter), (2) FM-labeling, and (3) inward calcium current and capacitance jump in responses to a depolarization pulse.

For both recordings, 1 μM TTX and 10 mM TEA-Cl were added to block Na^+ and K^+ channels. For slice recordings, 50 μM AP5 and 5 μM UBP310 were added to block NMDA and kainate receptors respectively in some experiments. Moreover, 100 μM CTZ was added to block desensitization of AMPA receptors. In some recordings, 50 μM forskolin was added. Recordings were performed at room temperature (20~25°C) within 4 hr after cutting the slices.

Whole-cell recordings

hMFBs were whole-cell voltage-clamped at −70 mV using EPC10/2 amplifier (HEKA, Germany), controlled by PatchMaster software (HEKA). The patch pipettes were filled with intracellular solution containing (in mM): 135 Cs-gluconate, 20 TEA-Cl, 10 HEPES, 5 Na_2-phosphocreatine, 4 MgATP, 0.3 GTP, and 0.5 EGTA (pH 7.2). In some experiments, EGTA was raised to 5 mM or was replaced with 5 mM BAPTA. When calcium imaging was performed, 0.1 Oregon Green 488 BAPTA-6F was added and EGTA was raised to 5 mM. Membrane currents were low-pass filtered at 3 kHz and sampled at 10 kHz. Data were analyzed offline with IgorPro software (Wavemetrics). Membrane capacitance measurements were performed using an EPC10/2 amplifier in the sine + DC configuration (Gillis, 2000). A sine wave (30 mV in amplitude, 1,000 Hz in frequency) was superimposed on a holding potential of −80 mV. Pipette (Harvard, GC150F-10) was coated with dental wax (dissociated) or not coated (slice) and had a resistance of typically ~10 MΩ (dissociated) or ~15 MΩ (slice). Average series resistance was ~20 MΩ (dissociated) or ~50 MΩ (slice). We stopped recordings when the leak currents exceeded 100 pA at resting potential. CA3 pyramidal cells were whole-cell clamped at −70 mV with a patch pipette (resistance of 3-5 MΩ). A series resistance was 5-20 MΩ, which was compensated so that residual resistance was < 5 MΩ. Liquid junction potential (10-15 mV) was not corrected. In some experiments, the EPSCs were evoked by stimulating the mossy fibers using a glass pipette (~3 MΩ).

For increasing the cAMP concentration in the presynaptic terminal, cAMP (0.5 mM) was directly dialyzed into the terminal via a recording patch pipette. Though such an experiment has not been done because of difficulty in direct patch clamp of the terminal, it has been well established that presynaptic cAMP is essential for inducing LTP at hMFBs (Nicoll and Schmitz, 2005). Moreover, extracellular application of forskolin (50 μM), a more conventional way to increase the presynaptic cAMP gave the same result, confirming that direct dialysis is valid.

TIRF microscopy

Cells were illuminated by TIRF on the stage of an inverted microscope (ECLIPSE TE2000-U, Nikon) equipped with a 100x oil immersion objective (NA1.49, Nikon). In our recording conditions, the decay constant of the evanescent field was ~100 nm (Midorikawa and Sakaba, 2015). A 488 nm laser (SAPPHIRE 488-20, Coherent) was used for FM1-43 excitation, and a 520 LP filter was used as an emission filter. Images were acquired every 30 ms using a sCMOS camera (Zyla, Andor), controlled by SOLIS software (Andor). Image magnification was 150x and provided 43 nm/pixel resolutions on the camera chip. Movies were acquired every minute. Voltage pulse and image capture were synchronized by a TTL pulse. Image analysis was performed using Metamorph (Universal Imaging), Excel (Microsoft) and Igor.

Given that our number of RRP vesicles was 68 from 92 sweeps (Figure 1), and a 100 ms depolarization induced ~30 fF (~400 vesicles) capacitance jump, it is estimated that ~0.2% of fused vesicles were observed as responders. By roughly assuming the TIRF illumination area as half of the entire membrane, the fraction of labeling can be estimated to be < 1%.

Analysis

Image analysis was performed using a combination of Metamorph (Universal Imaging), Excel (Microsoft), Igor, and MATLAB. Fluorescent spots within the footprint were first visually examined. Spots were rejected if they were unlikely to represent single synaptic vesicles; i.e., if they were blurred, too bright, oblong, or too large to be diffraction limited. After the selection, the remaining spots were Gaussian fitted to confirm that they were diffraction limited. To measure the fluorescence time course, the fluorescence of single vesicles was measured within a 344-nm circle centered on the vesicle. For Gaussian fitting of the vesicles, handmade program on the MATLAB was applied. All values were given as means ± SEM. Statistical significance was determined using the Student's t test.

The classification of synaptic vesicle events was performed as previously described (Midorikawa and Sakaba, 2015). In brief, "disappear" events were defined as those spots which showed sudden diminishing of the fluorescent spots. "bounce" events were defined as those spots which appeared and disappeared during the recording. "tether" events were defined as those spots which emerged in the middle of the recordings, and stayed stationary until the end of the given recording period (810 ms after the onset of depolarization).

Transmitter release rates have been calculated by deconvolving EPSCs with the mEPSCs (Diamond and Jahr, 1995; Neher and Sakaba, 2001), assuming the mEPSC amplitudes of ~40 pA. The mEPSC amplitudes have been measured by looking at asynchronous release events following the depolarizing pulse. The EPSCs were assumed to be linear summation of mEPSCs and have no residual currents due to delayed clearance of glutamate in the synaptic cleft (Neher and Sakaba, 2001). Validity of the calculated release rates was tested by comparing the cumulative release with capacitance jumps (Figure S2).

QUANTIFICATION AND STATISTICAL ANALYSES

Means and standard errors were calculated in Igor or Excel. p values were determined with Student's t test. Details, including sample sizes, can be found in figure legends.

Neuron, Volume *96*

Supplemental Information

Kinetics of Releasable Synaptic Vesicles and Their Plastic Changes at Hippocampal Mossy Fiber Synapses

Mitsuharu Midorikawa and Takeshi Sakaba

Supplemental information

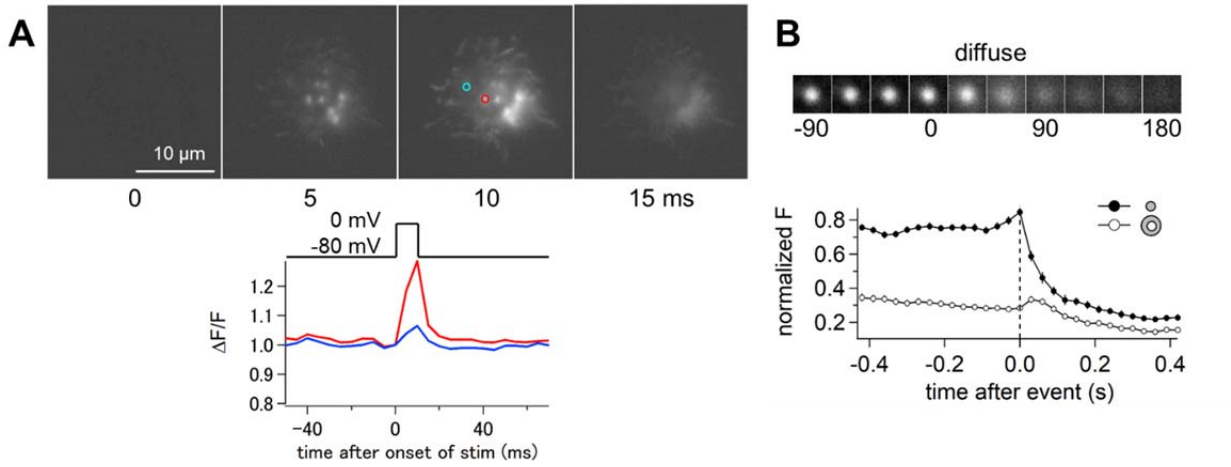

Figure S1 (related to Figure 1). Release sites at the TIRF surface are active, and elicit exocytosis.

A. The hMFB was loaded with Oregon green 488 BAPTA-6F (100 μM) and a 10 ms depolarizing pulse to 0 mV was applied. Top shows the sequential images and each image is shown as ΔF/F. Punctate bright spots appeared upon the depolarization suggesting that the active zone at the TIRF illuminated area is still functional. Bottom; Changes in fluorescence intensity for the circles shown in a top image. **B.** Subsets of disappear events showed the spreading of FM dye into the surrounding area. The top images are averages of 44 spots after background (averages of 240-300 ms after disappearance) subtraction. Bottom shows the fluorescence time course within a center (344 nm diameter) and a concentric annulus (344 nm inner and 860 nm outer diameters).

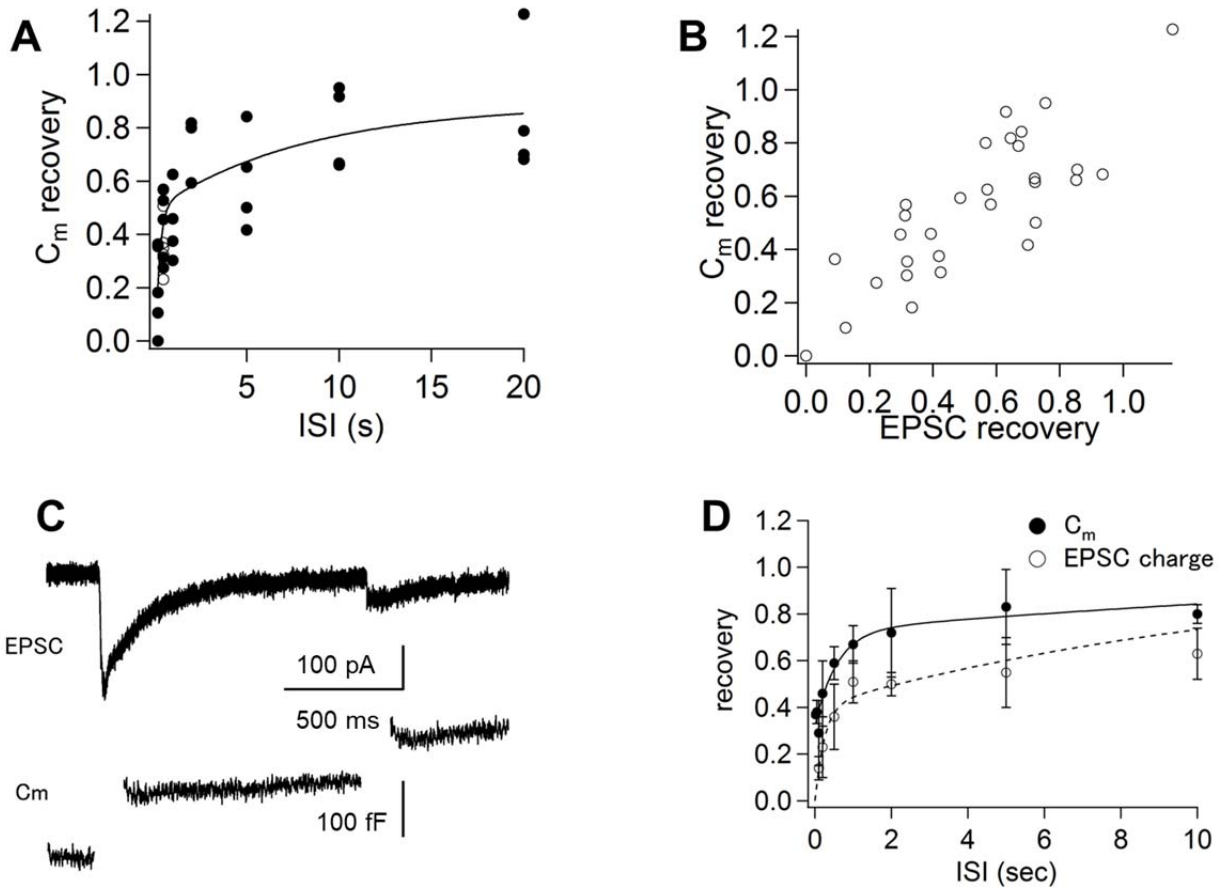

Figure S2 (related to Figure 3). Recovery time course of RRP measured by capacitance jumps and EPSCs in slices.

A. Simultaneous recordings of EPSC and membrane capacitance were performed at hMFB-CA3 synapses (Figure 3E). CTZ (100 μM) was added. A pair of 100 ms pulses was applied with varied intervals to monitor recovery of the RRP. The same data set as Figure 3E, but recovery of the capacitance response was plotted against the stimulus interval. **B.** Recovery of the capacitance response was plotted against that of cumulative release estimated from the EPSC deconvolution. Note the linear relationship between C_m and EPSC, indicating that the deconvolution is valid under CTZ. In **A**, we also plotted recovery of the RRP in the presence of

cAMP (open circles, ISI = 500 ms, 0.36 ± 0.04, n = 5 compared with 0.45 ± 0.05 in control). The result suggests that vesicle replenishment is not altered by cAMP. **C-D.** Similar experiments as Figure S2A, but CTZ was omitted from the extracellular solution. A pair of 100 ms pulses to 0 mV was applied with varied intervals to monitor recovery of the RRP. In **C,** the interval was 1 sec. In **D**, recovery of the capacitance (filled circles) and the EPSC integral (open circles) was plotted against the stimulus interval (n = 4 cell pairs). Note that the recovered fraction of the EPSCs was somewhat smaller, suggesting that AMPA receptor desensitization may contribute to the attenuation of synaptic currents when the released amounts were large.

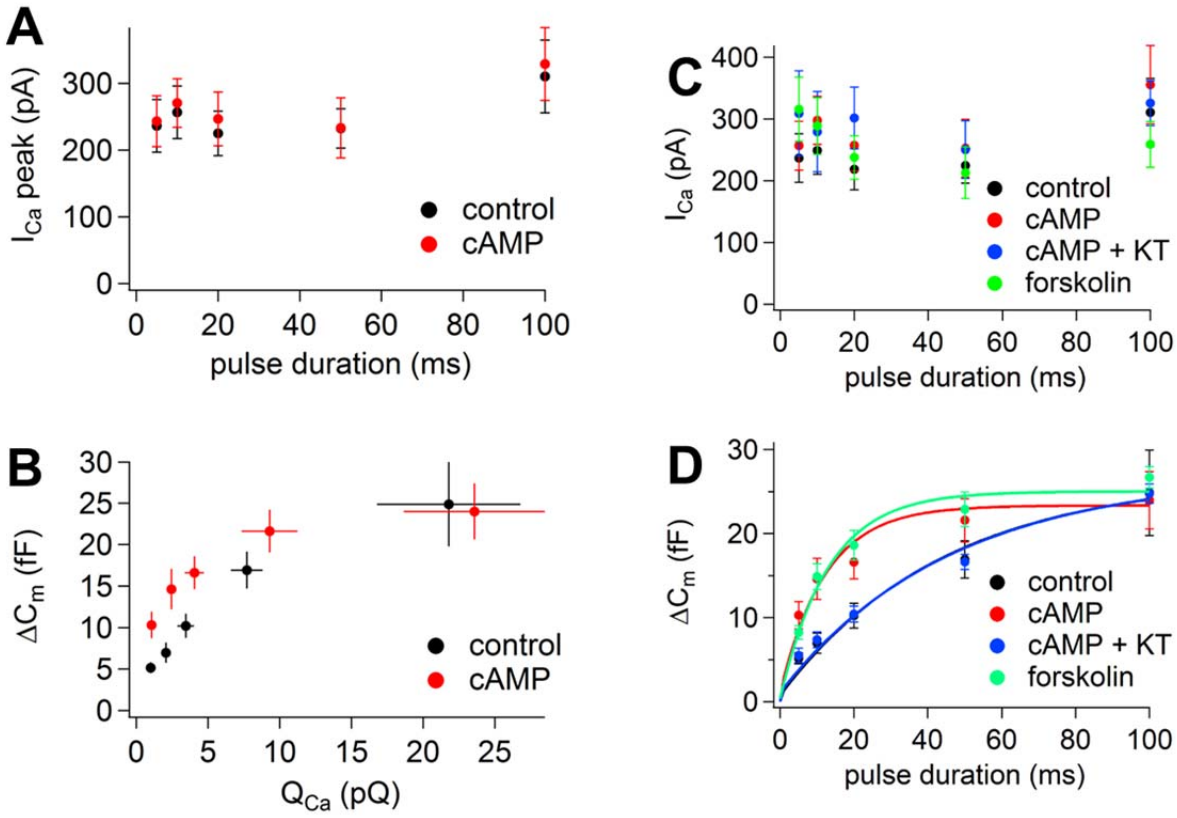

Figure S3 (related to Figure 4). Effect of cAMP on exocytosis

A. Peak amplitudes of Ca^{2+} currents recorded from dissociated hMFBs were plotted against the pulse duration for control (black) and cAMP (red) condition. **B.** The ΔC_m of the dissociated hMFBs were plotted against Q_{Ca} for control (black) and cAMP (red) condition. **C.** Peak amplitudes of Ca^{2+} currents recorded from dissociated hMFBs were plotted against the pulse duration for control (black), cAMP (red), cAMP + KT5720 (blue), and forskolin (green) condition. **D.** The ΔC_m of the dissociated hMFBs were plotted against the durations of depolarizations for control (black), cAMP (red), cAMP + KT5720 (blue) and forskolin (green) condition. Control and cAMP data are the same as in Figure 4B. cAMP + KT5720 condition, n = 5, 5, 7, 8, and 10 for 5, 10, 20, 50 and 100 ms, respectively; forskolin condition, n = 14, 14, 13, 13, and 12 for 5, 10, 20, 50 and 100 ms, respectively.

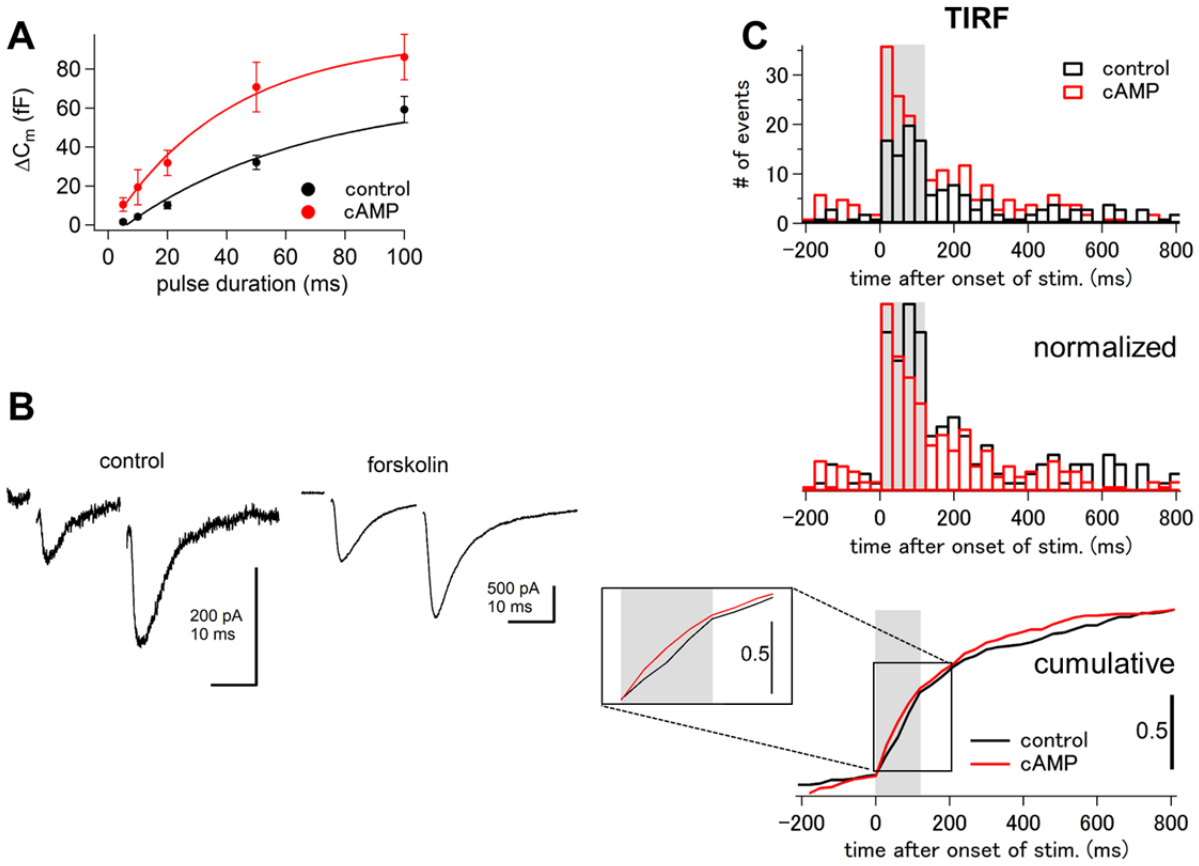

Figure S4 (related to Figure 4). Effect of cAMP on the exocytosis kinetics of hMFBs in slices and in TIRF imagings.

A. The ΔC_m of the hMFBs in slices were plotted against the duration of depolarization for control (black, the same as Figure 2C) and cAMP (red, n = 6 cells) condition. Exponential fits suggest that the RRP size and the release time constant were 67 fF and 61 ms under control condition, and 95 fF and 25 ms under cAMP condition, respectively. This suggests that a major change is the release time course rather than the RRP size. **B.** Mossy fibers were stimulated twice with an interval of 20 ms to evoke the EPSCs. Example traces before (control) and after application of forskolin (50 μM) are shown (average of 10-20 trials for each trace in the same cell). EPSCs were potentiated from 123 ± 82 pA to 706 ± 197 pA ($p < 0.01$, 5.25 ± 0.92-fold, n =7). Paired pulse ratio was changed from 2.05 ± 0.29 to 1.53 ± 0.24 ($p < 0.01$), consistent with

change in the release probability. **C.** Overlaid PSTHs of disappear events for control (black) and cAMP condition (red). Same datasets from Figure 1E and Figure 4C (top). In middle, the data are normalized to the peak in each condition. In bottom, the normalized cumulative histogram is shown. A 100 ms depolarization was applied at the time indicated by gray shading.